Nano Research
2023, 16(5): 7459–7469
ISSN 1998-0124 CN 11-5974/O4
https://doi.org/10.1007/s12274-022-5354-4

Research Article

Ultrasensitive and point-of-care detection of plasma phosphorylated tau in Alzheimer's disease using colorimetric and surface-enhanced Raman scattering dual-readout lateral flow assay

Liding Zhang[1,2,§], Ying Su[3,§], Xiaohan Liang[1,2], Kai Cao[1,2], Qingming Luo[4,5], and Haiming Luo[1,2,5] (✉)

[1] *Britton Chance Center for Biomedical Photonics, Wuhan National Laboratory for Optoelectronics, Huazhong University of Science and Technology (HUST), Wuhan 430074, China*
[2] *MoE Key Laboratory for Biomedical Photonics, School of Engineering Sciences, Huazhong University of Science and Technology, Wuhan 430074, China*
[3] *Department of Neurology, Union Hospital, Tongji Medical College, Huazhong University of Science and Technology, Wuhan 430074, China*
[4] *Key Laboratory of Biomedical Engineering of Hainan Province, School of Biomedical Engineering, Hainan University, Haikou 570228, China*
[5] *Research Unit of Multimodal Cross Scale Neural Signal Detection and Imaging, Chinese Academy of Medical Sciences, HUST-Suzhou Institute for Brainsmatics, Jiangsu Industrial Technology Research Institute (JITRI), Suzhou 215123, China*
[§] *Liding Zhang and Ying Su contributed equally to this work.*

Received: 4 September 2022 / **Revised:** 23 November 2022 / **Accepted:** 24 November 2022

ABSTRACT

Phosphorylation of tau at Ser (396, 404) (p-tau^{396,404}) is one of the earliest phosphorylation events, and plasma p-tau^{396,404} level appears to be a potentially promising biomarker of Alzheimer's disease (AD). The low abundance and easy degradation of p-tau in the plasma make the lateral flow assay (LFA) a suitable choice for point-of-care detection of plasma p-tau^{396,404} levels. Herein, based on our screening of a pair of p-tau^{396,404}-specific antibodies, we developed a colorimetric and surface-enhanced Raman scattering (SERS) dual-readout LFA for the rapid, highly sensitive, and robust detection of plasma p-tau^{396,404} levels. This LFA realized a detection limit of 60 pg/mL by the naked eye or 3.8 pg/mL by SERS without cross-reacting with other tau species. More importantly, LFA rapidly and accurately differentiated AD patients from healthy controls, suggesting that it has the potential for clinical point-of-care application in AD diagnosis. This dual-readout LFA has the advantages of simple operation, rapid, and ultra-sensitive detection, providing a new way for early AD diagnosis and intervention, especially in primary and community AD screening.

KEYWORDS

Alzheimer's disease, p-tau^{396,404}, plasma detection, surface-enhanced Raman scattering, lateral flow assay

1 Introduction

Alzheimer's disease (AD) is a complex pathophysiological neurodegenerative disease characterized by brain atrophy [1–3]. Unfortunately, given the limited efficacy of current AD treatments on symptoms, the number of AD patients worldwide is estimated to increase from the current estimate of 50 million to more than 152 million by 2050 [4, 5]. Given that neurodegenerative diseases are persistent and progressive, a longer preclinical phase brings the possibility of early AD diagnosis. The pathology of AD is characterized by senile plaques containing β-amyloid ($A\beta_{42}$) protein and neurofibrillary tangles (NFTs) composed of phosphorylated tau (p-tau), but it is difficult to pathologically identify AD in living individuals [5–8]. To date, autopsy histopathological examination of Aβ plaques and NTFs in the brain tissue is the only way to definitively confirm AD. Positron emission tomography (PET), magnetic resonance imaging (MRI), and cerebrospinal fluid (CSF) assessments have been used to detect the presence of AD lesions *in vivo* [9]. CSF testing is a highly invasive lumbar puncture with a limited number of samplings, and therefore, has an extremely negative perception among clinical AD patients, especially those at a high risk of developing AD [9, 10]. Because of the high cost and perceived invasiveness of these approaches, recent studies have focused on plasma-based AD biomarkers to diagnose and facilitate clinical trial recruitment [11]. Phosphorylation of tau at Ser (396, 404) (p-tau^{396,404}) is one of the earliest phosphorylation events, and is a major component of paired helical filaments (PHFs) and oligomer, resulting in the formation of pentangles [12, 13]. Increasing evidence confirms that ultrasensitive assays for tau phosphorylation at threonine 181 (p-tau^{181}), 231 (p-tau^{231}), and p-tau^{396,404} can identify the presence of brain NFTs and Aβ plaques *in vivo* and even predict the development of AD up to several years before clinical onset [14–19].

Blood tests have the advantages of simplicity, low-cost sampling, and non-invasiveness, allowing more frequent testing and screening in various relevant settings, including primary care, community health centers, and even at home [20, 21]. High levels

Address correspondence to hemluo@hust.edu.cn

of p-tau in the brain can be transmitted to the peripheral system via neurons [22], peripheral monocytes [23], axons [24–27], and exosomes [28, 29]. However, only a small fraction of p-tau enters the blood, which makes it difficult to measure the low-abundance p-tau that enters the blood in the matrix, as its concentration is usually at the picogram level [18, 30]. More than 85 phosphorylation sites on the tau protein of AD patients lead to the diversification of p-tau isoforms, posing a great challenge to the screening of phosphorylation-selective antibodies. Therefore, anti-p-tau^{396,404} antibodies directly determine the accuracy and specificity of diagnosis tools [19, 31, 32].

Currently, the detection of p-tau in the blood is mainly based on improved enzyme-linked immunosorbent assay (ELISA), such as the single-molecule counting (SMC™) immunoassay technology and Meso Scale Discovery (MSD) electrochemiluminescence immunoassay platform. While these methods can increase the sensitivity of conventional ELISA for the detection of p-tau levels in plasma by 20–100 folds, they are time-consuming and costly and require special equipment (Table 1) [33, 34]. For example, MSD assays require expensive MSD imagers and specially designed 96-well plates containing electrodes instead of plastic plates, resulting in high assay costs ($35 per sample). High detection costs and long testing time limit the application of these methods in the early diagnosis of AD in primary and community. Point-of-care testing (POCT) minimizes the time required to obtain clinically relevant results using simple devices, enabling clinicians and patients to make quick decisions. Colorimetric lateral flow assay (LFA) is an acceptable point-of-care (POC) diagnostic tool for the detection of p-tau levels in the plasma due to its low cost, reliability, and short assay time [35]. However, lack of quantification and low analytical sensitivity often hinder the application of this technique.

Table 1 Comparison of dual-readout LFA with other detection methods[a]

Method	Analyte	Cost	Time	Sensitivity	Ref.
Dual-readout LFA	p-tau^{396,404}	Low	0.5 h	3.8 pg/mL	This work
BSR-ELISA	p-tau^{396,404}	Moderate	15 h	5 pg/mL	[56]
SERS	p-tau$^{124/396}$	NA	NA	NA	[14]
Aptasensor	p-tau^{231}	Low	2.33 h	4.71 pg/mL	[57]
MSD	p-tau^{181}	High	5 h	1.4 pg/mL	[31]
Simoa	p-tau^{231}	High	5 h	2.2 pg/mL	[18]
ELISA	tau	Moderate	5 h	780 pg/mL	[58]

[a]BSR, bienzyme-substrate-recycle; NA, not available; Simoa, Single molecule array.

So far, various detection labels such as magnetic particles [36], fluorescent microspheres [37], Au–Ag [38], lanthanide [39], and upconversion nanoparticles [40] have been applied in LFA to address the issues of colorimetric LFA sensors. Among them, surface-enhanced Raman scattering (SERS) tags have high sensitivity and have gained popularity in both *in vivo* and *in vitro* diagnosis due to their excellent SERS activity and anti-interference ability [41–43]. Recently, SERS-based LFA sensors have been developed for the sensitive detection of several targets, including bacteria [44], DNA [45], toxins [46], hormones [47], cancer [48], and viruses [49]. However, the aforementioned SERS-LFA mainly focused on targets with higher stability in samples. In fact, due to its POC and ultrasensitive detection properties, SERS-LFA is an ideal diagnostic tool for some low-abundance, easily degradable plasma biomarkers such as p-tau^{181} and p-tau^{396,404}.

In this study, a colorimetric and SERS-based dual-mode lateral flow assay was successfully established for the POC and quantitative detection of p-tau^{396,404} in plasma. In this assay, the Roman signaling molecule 4-mercaptobenzoic acid (4-MBA) was modified on the surface of Au nanoparticles (AuNPs) to generate strong SERS signals. The phosphorylation-selective and high-affinity antibody 3G5 was then conjugated to 4-MBA@AuNP (4-MBA@AuNP-3G5) to capture soluble p-tau^{396,404}. The captured p-tau^{396,404}-4-MBA@AuNP-3G5 complex was migrated along the nitrocellulose (NC) membrane via chromatography and then immobilized by the corresponding paired antibody 4B1 sprayed on the test line. Test results can be observed with the naked eye and quantified based on the SERS intensity or the colorimetric value of the test line. To demonstrate the specificity of the dual-readout LFA, we tested the cross-reactivity of LFA with several plasma biomarkers, including p-tau^{231}, p-tau^{181}, p-tau^{217}, np-tau^{231}, and np-tau^{396,404}. Furthermore, we demonstrated the clinical utility of this LFA for the POC detection of p-tau^{396,404} in plasma samples of transgenic mice, AD patients, and healthy controls. Taken together, this is an example of successful sensitive detection of p-tau^{396,404} levels in clinical AD plasma samples using colorimetric and SERS dual-mode test strips.

2 Experimental

2.1 Materials and instrumentation

Different forms of tau peptides were custom-synthesized as lyophilized powders with a purity of > 95%. The sequences of the synthesized peptides are shown in Table S1 in the Electronic Supplementary Material (ESM). Human p-tau^{181} and p-tau^{217} ELISA kits were purchased from Jianglai Biotech Co., Ltd. (Shanghai, China). p-tau^{396,404}-specific monoclonal antibodies (mAbs) 3G5 and 4B1 were produced at our laboratory [17]. Dehydrated trisodium citrate ($HAuCl_4$), 4-MBA, and bovine serum albumin (BSA) were purchased from Sigma Aldrich (St. Louis, MO, USA). Filter paper and semi-rigid polyvinyl chloride (PVC) sheets were obtained from Jieyi Biological Technology Co., Ltd. (Shanghai, China). Glass fiber membranes and nitrocellulose membranes were obtained from Millipore (Billerica, MA, USA). Horseradish peroxidase (HRP)-conjugated or unconjugated goat anti-mouse IgG was ordered from GenScript (Nanjing, China). Protein A/G magnetic beads were gifted by LinkedIn Biotechnology Co., Ltd. (Shanghai, China). Prestained protein marker and high sensitivity enhanced chemiluminescence (ECL) chemiluminescence detection kit were ordered from Vazyme, Biotech Co., Ltd. (Nanjing, China).

Transmittance electronic microscopy (TEM) images were obtained using a Tecnai G20 transmission electron microscope (FEI Ltd., USA) at a voltage of 200 kV. Dynamic light scattering was performed on the Zetasizer Nano ZS90 equipment (Malvern Instruments, UK). Further, Raman spectra were collected from 900 to 1,200 cm^{-1} with a 50× objective lens (N.A. = 0.75, WD = 0.37 mm), with a total of 3 points per sample measured using a Raman microscope system (Horiba Jobin-Yvon LabRAM HR800, Germany) operated at λ = 785 nm. The laser power was set at 100 mW and the integration time was 15 s.

2.2 Preparation of AuNPs and SERS nanoprobes

1 mL of 1% chloroauric acid solution was added to 99 mL of deionized water, and then the mixture was heated with stirring. After 15 min of heating, 1 mL of 1% trisodium citrate was added when the solution began to boil slightly. A few minutes later, the color of the solution gradually changed from colorless to gray, black, purple, and finally red. Keeping the solution boiling, heating was continued for 20 min to obtain 40 nm colloidal gold [50, 51].

Synthetic AuNPs were added with carbonate buffer (12 μL,

0.1 M K_2CO_3), and then 15 μL of 4-MBA (1 mM) and 15 μg of anti-p-tau^{396,404} mAb 3G5 were added and allowed to react for 30 min at room temperature. After incubation, the mixture was centrifuged at 11,000× *g* for 15 min to remove excess 4-MBA and mAb 3G5. Subsequently, 10 μL of 20% BSA dissolved in tris-buffered saline (TBS, 20 mM Tris and 137 mM NaCl, pH 7.6) was added to the 4-MBA@AuNP-3G5 conjugate solution and incubated at room temperature for 1 h to block naked 4-MBA@AuNP. Finally, 4-MBA@AuNP-3G5 conjugates were collected and washed three times with TBS to remove unbound reagents. The prepared 4-MBA@AuNP-3G5 conjugate was resuspended and stored in a storage buffer (TBS, pH 8.4, including 0.05% protein stabilizer, 1% BSA, 0.1% poly(vinyl pyrrolidone) (PVP), 1% NaN_3, 0.1% polyethylene glycol (PEG), and 0.05% Tween-20) at 4 °C for further use.

2.3 Dual-readout LFA preparation

Figure 1 describes the main components of integrated LFA, mainly including the sample pad, the nitrocellulose membrane (sprayed with T-line and control line (C-line)), and the absorption pad assembled in sequence on a plastic backplane. Sample pads were pretreated with TBS containing 1% BSA (w/v), 2% sucrose (w/v), 0.1% PEG (v/v), and 0.05% Tween-20 (v/v), and then dried at 60 °C. The T-line and C-line were sprayed on the surface of nitrocellulose membranes with anti-p-tau^{396,404} 4B1 (1 mg/mL) and goat anti-mouse antibody (1 mg/mL), respectively. The assembly sequence of LFA was as follows: The sample pad was first placed on the PVC plate, overlapping the NC membrane by 2 mm, and then affixed 2 mm near the absorbent pad. After assembly, the plate was evenly cut into 3-mm-wide strips, sealed with desiccant, and stored at room temperature for later use.

2.4 Optimization of key parameters

To ensure optimal detection sensitivity of LFA, we optimized the volumes of 4-MBA and K_2CO_3 and the concentration of 3G5. To optimize the volume of 4-MBA, 5, 10, 15, and 20 μL of 4-MBA (1 mM) were added to 1 mL of AuNP solution. The SERS intensity of 4-MBA@AuNP in each volume was detected by the labRAM HR800. To optimize the volume of K_2CO_3, 4, 8, 12, 16, 20, 24, 28, and 32 μL of 0.1 M K_2CO_3 were added to 1 mL of AuNP solution, and the absorbance was detected at 525 nm. For determining the optimal loading of 3G5, 3G5 was added dropwise to 1 mL of AuNP solution for obtaining final concentrations of 5, 10, 15, 20, 25, and 30 μg/mL.

2.5 Detection principle and test procedure of dual-readout LFA

The prepared dual-readout LFA system developed for rapid and visual detection of p-tau^{396,404} was based on a set of paired antibodies. Because mAb 3G5 specifically and selectively binds to p-tau^{404}, whereas mAb 4B1 specifically and selectively binds to both p-tau^{396} and p-tau^{404}, the paired antibody enables the detection of p-tau^{396,404}.

The dual-readout LFA assay procedure includes the following steps: 30 μL of 3G5-modified 4-MBA@AuNP (4-MBA@AuNP-3G5) was used to capture p-tau^{396,404} dissolved in the sample, and was then dripped onto the sample pad. Further, 4-MBA@AuNP-3G5-p-tau^{396,404} in the samples migrated along the NC membrane and was immobilized with mAb 4B1 sprayed on the NC membrane to form the T-line, whereas the remaining 4-MBA@AuNP-3G5 continued to migrate until it was immobilized by goat anti-mouse IgG sprayed on NC membrane to form the C-line. Test results were evaluated by the signal intensity of the color or SERS on the T-line.

2.6 Sensitivity and specificity of dual-readout LFA

A series of concentration gradients from 125 ng/mL to 3.8 pg/mL of p-tau^{396,404} solutions were prepared using TBS buffer. Antigen enrichment was performed using 4-MBA@AuNP-3G5 in the solution. Subsequently, the enriched antigen was loaded onto the sample pad of the test strip. Following this, the signal intensity on the T-line was analyzed by SERS. Under optimal conditions, a standard curve was established by plotting the signal intensity on the T-line with a series of p-tau^{396,404} concentrations. LFA specificity was evaluated by testing several different tau proteins, including p-tau^{231}, p-tau^{181}, p-tau^{217}, np-tau^{396,404}, and np-tau^{231} at 50 ng/mL; 5 ng/mL of p-tau^{396,404} was used as the positive control and PBS was used as the blank control.

2.7 Detection of plasma samples using dual-readout LFA

To evaluate the reliability of LFA, 26 plasma samples were collected from 3- (n = 3) and 9-month-old 5xFAD (n = 3) and age-

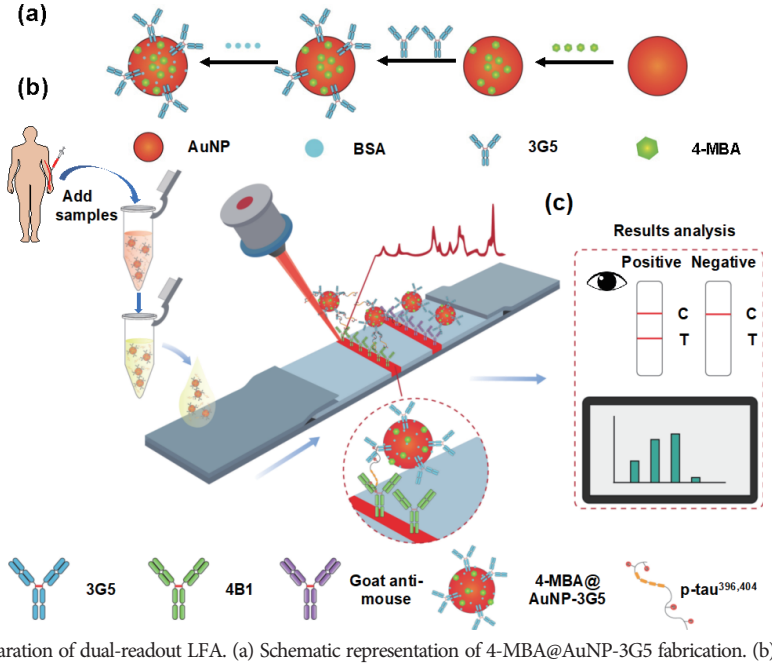

Figure 1 Flow chart for the preparation of dual-readout LFA. (a) Schematic representation of 4-MBA@AuNP-3G5 fabrication. (b) Separation and enrichment of p-tau^{396,404}, following the loading of immunocomplexes onto the lateral flow test strips. (c) Imaging and interpretation of results.

matched C57BL/6J (n = 6), AD patients (n = 6) and healthy individuals (n = 7) and detected by LFA. All procedures involving animal studies were reviewed and approved by the Institutional Animal Care and Use Committee of Huazhong University of Science and Technology. Details of the participants are summarized in Table S2 in the ESM. Dual-readout LFA was performed as described above.

2.8 Dot blot and ELISA

For Dot blot, 1 μg of p-tau^{396}, p-tau^{404}, np-tau^{396}, and np-tau^{404} were pipetted onto poly(vinylidene fluoride) (PVDF) membranes and blocked in 5% skimmed milk with TBS buffer containing 0.05% Tween-20 (TBS-T) at room temperature for 1 h. The membranes were then incubated with 3G5 and 4B1 (1:1,000), followed by secondary antibody HRP-conjugated goat anti-mouse IgG (H+L) (1:8,000). After each step, the membrane was washed three times in TBS-T. Finally, immunological signals were detected with high sensitivity ECL chemiluminescence detection kit using Tanon 5200 Muiti (Shanghai, China).

For indirect ELISA, each well of a 96-well plate (NEST Biotechnology Co., Ltd., Wuxi, China) was coated with 0.5 μg of p-tau^{396,404} diluted in citrate-buffered saline (CBS, 14.2 mM Na_2CO_3 and 34.8 mM $NaHCO_3$, pH 9.6) overnight at 4 °C. All wells were blocked with 5% skimmed milk dissolved in TBS-T at 37 °C for 2 h. Next, the primary antibodies of 3G5 and 4-MBA@AuNP-3G5 at the same concentration were added to incubate with coated antigens in each well at 37 °C for 2 h. HRP-conjugated goat anti-mouse (1:8,000) was added to the plate and incubated for 1 h at 37 °C. The plate was washed four times with TBS-T in each step. A highly sensitive soluble 3,3'5,5'-tetramethylbenzidine (TMB) substrate solution (Abcam) was added to detect the immunoreaction and then stopped with 2 M H_2SO_4. An Epoch microplate spectrophotometer (Bio Tek, USA) was used to analyze the plates at 450 nm.

For p-tau^{181} and p-tau^{217} detection, human plasma samples were collected and detected by the commercial ELISA kits, according to the manufacturer's introductions.

2.9 Tissue imaging

Coronal cryosections of 3- and 9-month-old 5xFAD mouse brains were blocked with 3% bovine serum albumin in TBS buffer containing 0.2% Triton X-100 for 2 h at 25 °C, and then incubated with Cy3-labeled anti-Aβ_{42} mAb 1F12 [52, 53] and fluorescein isothiocyanate (FITC)-conjugated anti-p-tau^{396,404} mAb 3G5 or 4B1 [17] overnight at 4 °C. Subsequently, the slides were washed five times with TBS and stained with 6-diamino-2-phenylindole (DAPI; Thermo Fisher Scientific). All fluorescence signals were detected using a Zeiss LSM710 microscope.

2.10 Statistical analyses

The intensity of the T line in colorimetric mode was obtained by scanning the strips and quantified with ImageJ [54]. Data are presented as mean ± standard deviation (SD). Unpaired t-tests were used to compare multiple groups. One-way analysis of variance (ANOVA) was used for multigroup comparisons. Statistical significance is represented in figures by $^*p < 0.05$. All statistical analyses were performed using the GraphPad Prism 8.0 software.

3 Results and discussion

3.1 Principle of colorimetry and SERS dual-readout LFA

The poor detection sensitivity of LFA is one of the main reasons limiting its application for the detection of low-level biomarkers in plasma. Herein, we propose that a dual-readout LFA using a pair of high-affinity antibodies coupled with SERS can significantly improve the LFA detection sensitivity. As shown in Fig. 1(a), the AuNP was prepared and modified with Roman signaling molecule 4-MBA, which was then conjugated with phosphorylation selective antibody 3G5. The prepared 4-MBA@AuNP-3G5 was used to recognize and capture responding antigens, and then loaded onto the lateral flow strips and subsequently recognized by 4B1 sprayed on the T-line, forming sandwich immunocomplexes and accumulating to produce a red line (Fig. 1(b)). Uncaptured 4-MBA@AuNP-3G5 complexes were subsequently immobilized in the control area by secondary antibodies to generate a C-line. If a sample did not contain p-tau^{396,404}, all uncaptured 4-MBA@AuNP-3G5 complexes were immobilized in the control area by the secondary antibody to generate a C-line. The detection results can be judged by visual observation of the color intensity of the aggregated AuNPs or by quantitative analysis of the SERS signal intensity, both of which are proportional to the sample concentration (Fig. 1(c)).

3.2 Characterization of 3G5 and 4B1 antibodies

Phosphorylation-selective antibodies were obtained by fusing B cells and SP2/0 cells followed by screening with ELISA and immunofluorescence using the limiting dilution method as described previously (Fig. 2(a)) [55]. mAbs 3G5 and 4B1 were selected for the dual-readout LFA. The isotype of 3G5 and 4B1 was determined as IgG1 (Table S3 in the ESM). The purity and molecular weight of 3G5 and 4B1 were identified by 12% reduced sodium dodecyl sulfate-polyacrylamide gel electrophoresis (SDS-PAGE) gels (Fig. 2(b)). ELISA results showed high binding affinity of 3G5 and 4B1 toward p-tau^{396,404} with K_d = 2.06 ± 0.037 nM for 3G5 (Fig. 2(c)) and K_d = 0.16 ± 0.022 nM for 4B1 (Fig. 2(d)). Both mAbs had titers as high as 10^6, with IC_{50} values of 49 and 14 nM for 3G5 and 4B1, respectively (Table S3 in the ESM). The bioactivity of the antibody pair was characterized by immunofluorescence and dot-blot assay. Immunostaining results showed that mAbs 3G5 and 4B1 could well recognize p-tau^{396,404} aggregates in the brain of 5xFAD mice (Fig. 2(e)). In addition, the dot-blot assay showed that 3G5 binds to p-tau^{404}, and 4B1 binds to p-tau^{396} and p-tau^{404}, exhibiting two epitopes. Furthermore, the two mAbs did not show any binding to non-Ser(P)-396/404 peptides (Fig. 2(f), bottom), indicating that both 3G5 and 4B1 are phosphorylation-selective.

3.3 Biomodification of SERS nanoprobe

The synthesized AuNPs exhibited a characteristic color of red wine, and a single absorption peak at 525 nm (Fig. S1(a) in the ESM and Fig. 3(a)). The morphology and size of the prepared AuNPs were characterized by TEM and dynamic light scattering, and the size was approximately 30–40 nm with good dispersion and homogeneity (Figs. 3(b) and 3(c)).

To prepare SERS nanoprobes, a layer of Raman molecules (4-MBA) was grafted onto the surface of AuNPs to form 4-MBA@AuNPs through a covalent bond between Au and the sulfhydryl groups of 4-MBA. The prepared 4-MBA@AuNPs were further modified with 3G5. After conjugation with 3G5, the hydrodynamic size of 4-MBA@AuNP-3G5 increased significantly from 40 nm to approximately 70 nm, and the Zeta potential also increased (Figs. 3(c) and 3(d)). Besides, the absorption spectrum of 3G5 was measured, resulting in a decrease in the absorption peak at 280 nm after conjugation with 4-MBA@AuNP (Fig. S2(a) in the ESM). In the ultraviolet–visible (UV–vis) spectrum shown in Fig. 3(a), the absorption peaks of 4-MBA@3G5-AuNPs showed a slight red shift compared with those of 4-MBA@AuNPs, indicating that part of the antibody was modified on 4-

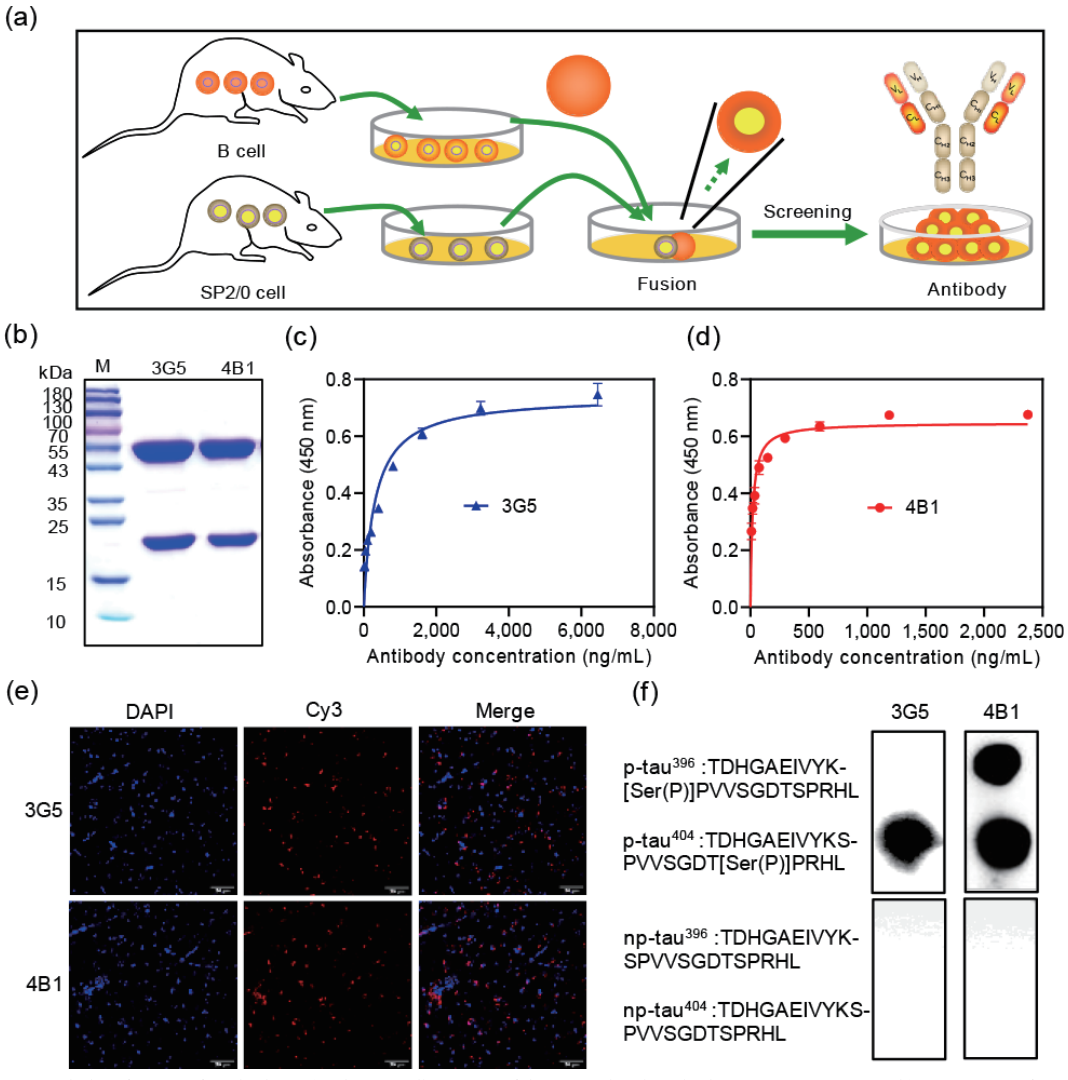

Figure 2 Screening and identification of antibodies. (a) Schematic illustration of the monoclonal antibody preparation process. (b) SDS-PAGE of purified mAbs 3G5 and 4B1. Binding affinities of 3G5 (c) and 4B1 (d) toward p-tau^{396,404}. (e) Confocal fluorescence images of p-tau^{396,404} aggregates in 5xFAD mouse brain slices stained with Cy3-labeled 3G5 and 4B1. (F) Phosphorylation sites of p-tau^{396,404} as recognized by 3G5 and 4B1. Data are presented as means ± SD, $n = 3$.

MBA@AuNP. Furthermore, 12% reduced SDS-PAGE showed that 3G5 was successfully coupled with 4-MBA@AuNPs presenting typical light and heavy chains of antibody (Fig. S2(b) in the ESM). Figure 3(e) shows characteristic bands of 4-MBA@AuNP-3G5 at 1,076 and 1,567 cm^{-1}. To evaluate the SERS enhancement effect of 4-MBA@AuNP-3G5, we compared the Raman intensities of 4-MBA@AuNP-3G5 and free 4-MBA at the same concentration. Interestingly, 4-MBA@AuNP-3G5 had a strong SERS signal, whereas free 4-MBA and AuNPs generated no measurable signal (Fig. 3(e)). Compared with 4-MBA and AuNPs, 4-MBA@AuNP-3G5 showed a SERS intensity value enhanced by approximately 767 and 2,545 folds, respectively, indicating that AuNP greatly enhanced the Raman intensity of 4-MBA (Fig. 3(f)). The most intense band of 4-MBA@AuNP-3G5 at 1,076 cm^{-1} was used for quantitative analysis because of its good resolution. The dissociation constant of 4-MBA@AuNP-3G5 (2.88 ± 0.087 nM) was slightly lower than that of 3G5 (2.06 ± 0.037 nM), indicating that 4-MBA@AuNP had little effect on the binding affinity of 3G5 to p-tau^{396,404} (Figs. 3(g) and 3(h)). The immunoprecipitation followed by reduced SDS-PAGE experiments was performed to evaluate the performance of 4-MBA@AuNP-3G5 to enrich p-tau^{396,404} in the plasma. The results showed that 4-MBA@AuNP-3G5 could identify and capture p-tau^{396,404} in spiked samples (Fig. 3(i)).

3.4 Optimization of dual-readout LFA working conditions

To achieve the highest sensitivity of LFA, the working conditions of LFA were optimized. The optimal loading of 4-MBA was first optimized, directly affecting the SERS signal intensity of 4-MBA@AuNP-3G5. As shown in Fig. S3 in the ESM, the SERS intensity increased on 4-MBA loading, but it stabilized when the added volume of 4-MBA was 15 μL, indicating that AuNPs were fully loaded with 4-MBA.

Next, the optimal volume of K_2CO_3 was optimized, which was a commonly used buffer for adjusting the pH of AuNP solutions for better antibody binding. The results showed that when the volume of 0.1 M K_2CO_3 increased from 4 to 12 μL, the optical density at 525 nm (OD_{525}) increased from 0.38 to 0.67, and the absorption spectral intensity gradually increased (Fig. S4(a) in the ESM). When the volume of 0.1 M K_2CO_3 was increased from 16 to 32 μL, the OD_{525} value (Fig. S4(a) in the ESM) and absorption spectrum intensity (Fig. S4(b) in the ESM) began to decrease. To obtain a higher colorimetric ratio, 12 μL of 0.1 M K_2CO_3 was chosen as the optimal volume for antibody conjugation.

The number of antibodies conjugated to AuNPs also affects the aggregation of AuNPs and the sensitivity of SERS-based immunoassays. As the concentration of 3G5 increased from 5 to 15 μg/mL, the OD_{525} value of the 4-MBA@AuNP-3G5 solution gradually increased from 0.37 to 0.643 (Fig. S5(a) in the ESM). However, when the concentration of 3G5 was further increased

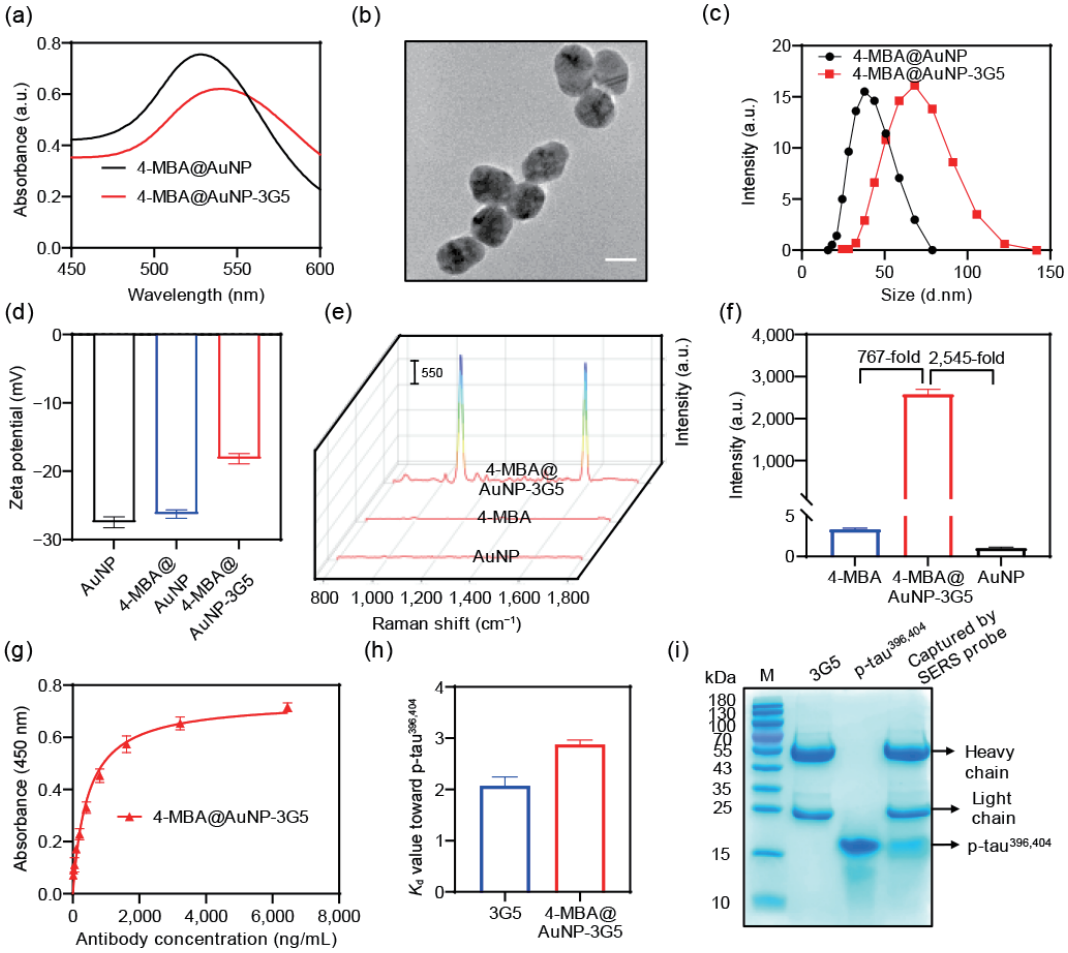

Figure 3 Preparation of Raman nanoprobes. (a) UV–vis absorption spectra of 4-MBA@AuNP before and after 3G5 conjugation. (b) TEM image of the synthetic AuNPs. Scale bar: 20 nm. (c) Size distribution of AuNPs before and after modification. (d) ζ-potential of AuNPs before and after modification. Raman spectra (e) and intensity (f) of 4-MBA@AuNP-3G5, 4-MBA, and 3G5. ((g) and (h)) The binding affinity of 4-MBA@AuNP-3G5 to p-tau^{396,404}. (i) p-tau^{396,404} in spiked samples was enriched with 4-MBA@AuNP-3G5 and visualized via SDS-PAGE. Data are presented as means ± SD, $n = 3$.

from 20 to 30 μg/mL, we observed a sharp drop in OD_{525} value (Fig. S5(a) in the ESM) and absorption spectrum intensity (Fig. S5(b) in the ESM). Therefore, to maintain the stability of AuNPs, 15 μg/mL was chosen to be the optimal concentration of 3G5.

Given that LFA is ultimately tested on plasma samples, the salt ion factor is also considered. However, the increase in the concentration of salt ions such as NaCl interferes with AuNP stability and leads to aggregation. Therefore, the stability of the 4-MBA@AuNP-3G5 solution was evaluated by adding different concentrations of NaCl (150 to 1,500 mM). When NaCl concentration was lower than 900 mM, the OD_{525} value (Fig. S6(a) in the ESM) and absorption spectrum (Fig. S6(b) in the ESM) of the 4-MBA@AuNP-3G5 solution showed no obvious change. However, when the NaCl concentration reached 1,200 mM, the OD_{525} value and absorption spectrum of the 4-MBA@AuNP-3G5 solution started to decrease (Fig. S6 in the ESM). With a further increase in the NaCl concentration, the OD_{525} value and absorption spectrum of 4-MBA@AuNP-3G5 significantly decreased (Fig. S6 in the ESM). These results indicated that 4-MBA@AuNP-3G5 could withstand relatively high salt buffer environments. Thus, the plasma NaCl concentration of approximately 142 mM is acceptable for 4-MBA@AuNP-3G5 given its salt tolerance of over 1,200 mM.

3.5 Specificity and sensitivity of dual-readout LFA

The performance of dual-readout LFA was evaluated under optimal experimental conditions. The specificity of LFA was tested using five different tau species, including p-tau^{231}, p-tau^{181}, p-tau^{217}, np-tau^{231}, and np-tau^{396,404}. Further, p-tau^{396,404} and PBS were used as positive and blank controls, respectively. In the colorimetric mode, the red T-line was only observed in the presence of p-tau^{396,404}, but not in the presence of p-tau^{231}, p-tau^{181}, p-tau^{217}, np-tau^{231}, and np-tau^{396,404} samples (Figs. 4(a) and 4(b)). Similarly, in the SERS mode, the characteristic bands of 4-MBA were detected at only 1,076 cm^{-1} (Fig. 4(c)). However, no SERS signal was detected in other tau species, indicating the high specificity of LFA (Figs. 4(c) and 4(d)).

Different concentrations of p-tau^{396,404} standard solutions, ranging from 3.8 pg/mL to 125 ng/mL, were used to evaluate the detection ability of dual-readout LFA. In the colorimetric mode, the cut-off value for LFA was defined as the minimum p-tau^{396,404} concentration at which the color on the T-line is completely invisible. As shown in Fig. 5(a), the color intensity on the T-line gradually weakens with the decrease in p-tau^{396,404} concentration. The results showed that the visual detection limit for p-tau^{396,404} was 60 pg/mL and the upper limit of detection was 125 ng/mL. Figure 5(b) and Fig. S7(a) in the ESM showed nonlinear and linear standard curves between T-line color intensity in LFA and p-tau^{396,404} concentrations ranging from 60 pg/mL to 125 ng/mL, respectively. In SERS mode, the Raman signal showed a good response with increasing p-tau^{396,404} concentration from 3.8 pg/mL to 125 ng/mL (Fig. 5(c)), exhibiting a good and wide nonlinear and linear range (Fig. 5(d) and Fig. S7(b) in the ESM). Notably, the limit of quantification of SERS-based LFA was as high as 3.8 pg/mL, which was approximately 16-fold higher than that observed in the colorimetric mode, indicating the significant

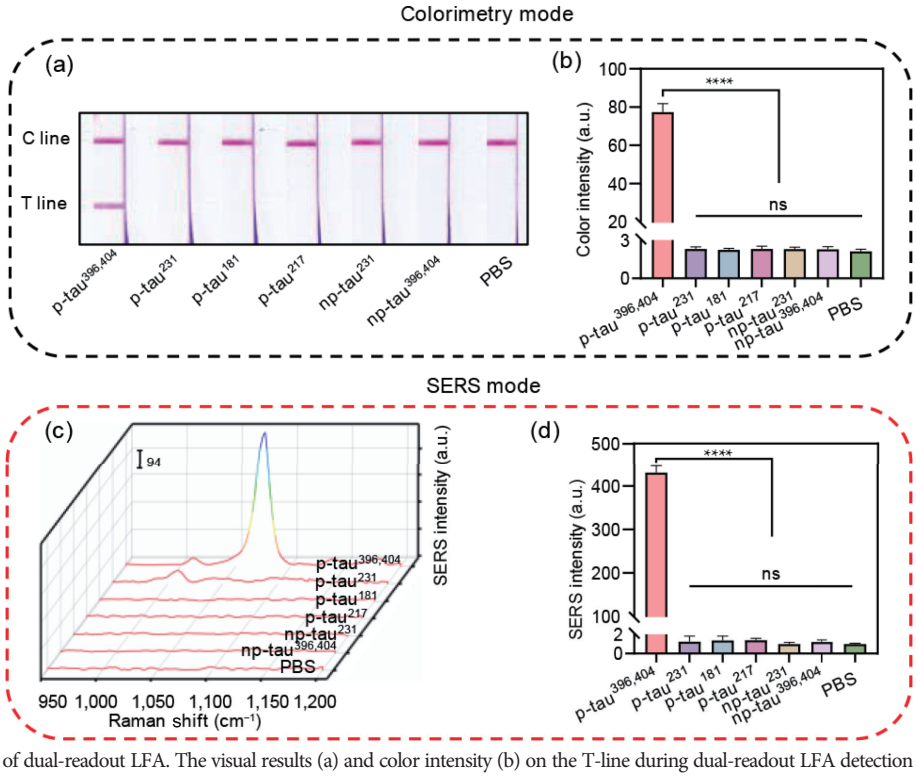

Figure 4 The selectivity of dual-readout LFA. The visual results (a) and color intensity (b) on the T-line during dual-readout LFA detection of different tau species in colorimetric mode. Raman spectra (c) and intensity (d) on the T-line during LFA detection of different tau species in SERS mode. Data are presented as means ± SD, $n = 3$. Statistical significance is indicated in the figures by $^{****}p < 0.0001$ and ns (indicating no significance).

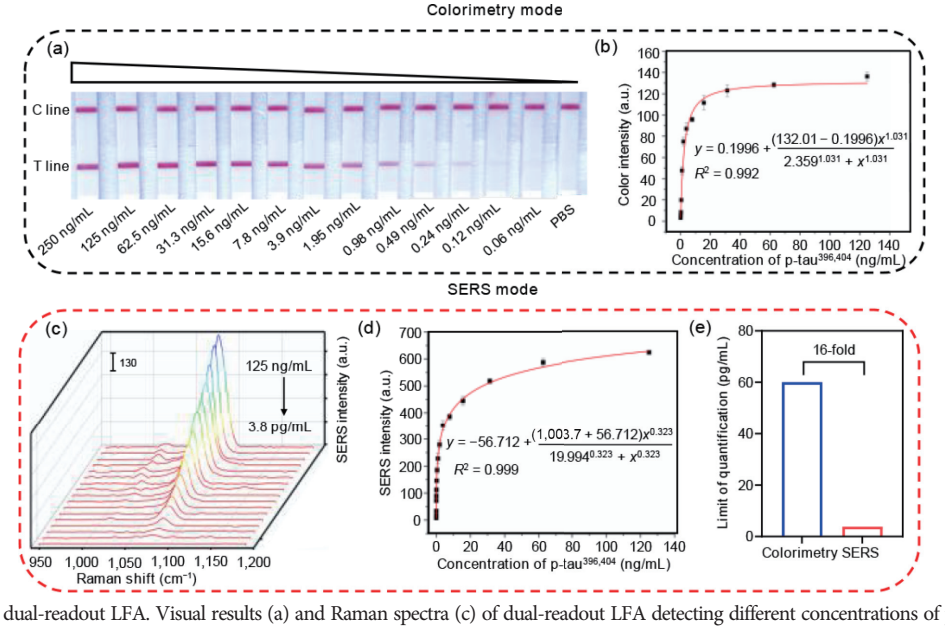

Figure 5 Selectivity of dual-readout LFA. Visual results (a) and Raman spectra (c) of dual-readout LFA detecting different concentrations of p-tau^{396,404} on the T-line. The nonlinear curve of T-line color (b) and SERS (d) intensity versus different p-tau^{396,404} concentrations. (e) Comparison of the limit of quantification between colorimetric and SERS modes. Data are presented as means ± SD, $n = 3$.

enhancement of the Raman signal and good performance of LFA in SERS mode (Fig. 5(e) and Table 1).

3.6 Performance evaluation of dual-readout LFA for the detection of plasma samples

Considering the encouraging sensitivity and selectivity of dual-readout LFA toward p-tau^{396,404}, we further evaluated its performance in plasma samples. We first evaluated the performance of LFA in the plasma samples of 3- or 9-month-old AD transgenic mice (5xFAD) or control mice (C57BL/6J) (n = 3 per group). The results showed that p-tau^{396,404} was detected in the blood of 3- and 9-month-old 5xFAD mice, but not in the plasma of age-matched C57BL/6J mice (Fig. 6(a)). The LFA results in colorimetric or SERS mode showed that the level of p-tau^{396,404} in the plasma of 9-month-old 5xFAD mice was significantly higher than that in the plasma of 3-month-old 5xFAD mice (Figs. 6(a)–6(c)). This phenomenon may be explained by the fact that 9-month-old 5xFAD mice are in a more severe stage with more p-tau^{396,404} and Aβ plaque burden compared with 3-month-old 5xFAD mice (Fig. 6(e)), increasing blood p-tau^{396,404} levels. We further found that the T-line color intensity in the plasma of 5xFAD mice was approximately 17.1 times stronger than that in C57BL/6J mice. However, in the SERS mode, the SERS intensity of the T-line in 5xFAD mice was approximately 112.8-fold higher than that in C57BL/6J mice, which was further 6.6-fold higher than that observed in the colorimetric mode, indicating SERS has

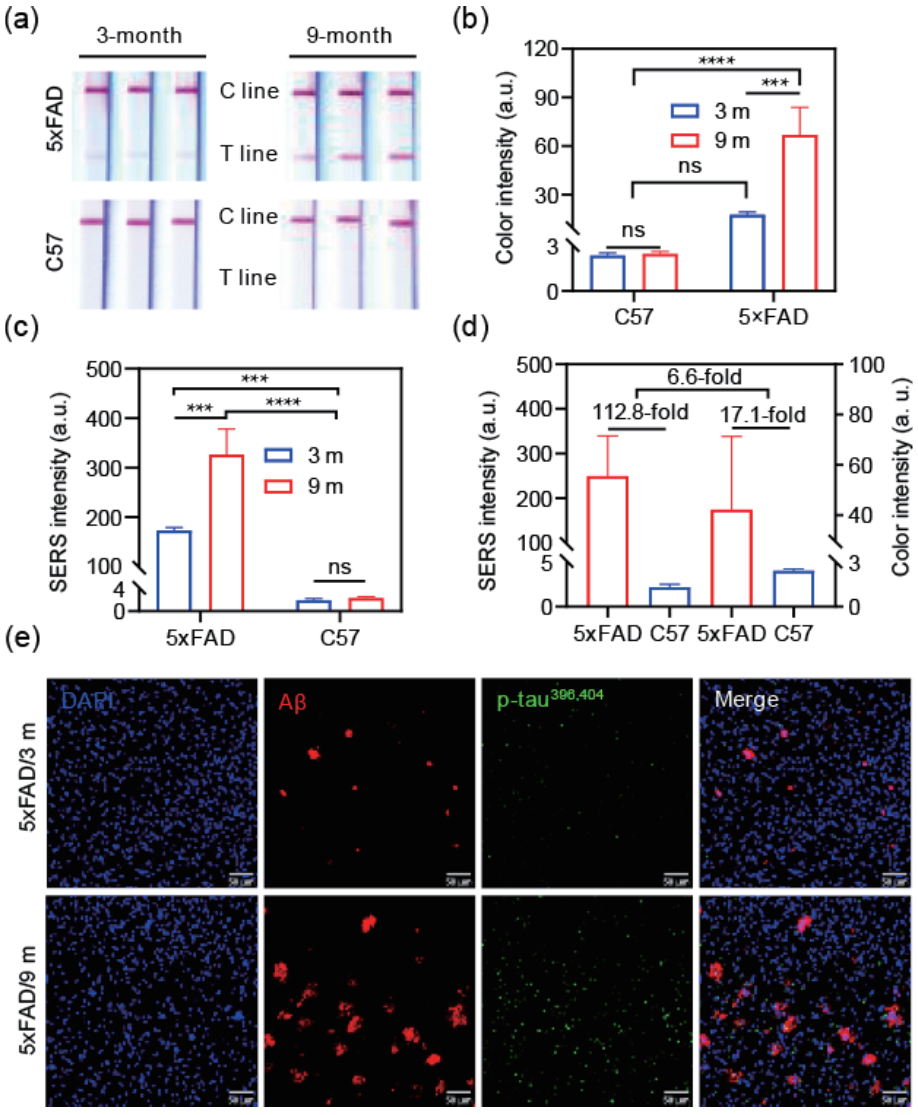

Figure 6 Performance of dual-readout LFA in mouse plasma samples. (a) The visual result of LFA in plasma samples of 3- and 9-month-old 5xFAD and C57 mice. Colorimetric (b) and SERS (c) intensity on T-line for the detection of plasma samples of 3- and 9-month-old 5xFAD and C57BL/6J (C57). (d) Comparison of 5xFAD to C57 plasma intensity ratios at 3 and 9 months of age in colorimetric and SERS modes. (e) Confocal fluorescence images of Aβ plaque and p-tau^{396,404} staining in 3- or 9-month-old 5xFAD mice. Data are presented as means ± SD, $n = 3$. Statistical significance is indicated in the figures by ***$p < 0.001$, ****$p < 0.0001$, and ns (indicating no significance).

extremely strong sensitivity and anti-interference ability (Fig. 6(d)).

In addition to mouse plasma samples, we also tested human plasma samples, including healthy controls (n = 7) and AD patients (n = 6). The results showed that red T-lines were observed with naked eyes in AD patients but not in healthy controls in colorimetric mode (Fig. 7(a)). Similar results were observed in the SERS mode. SERS spectra were found to be higher in AD patients than in the healthy control group (Fig. 7(b)). More importantly, the p-tau^{396,404} in AD patient and healthy controls plasma could be differentiated, and the results were identical to those obtained from the clinical diagnosis (Fig. 7(c), and Fig. S8 and Table S2 in the ESM). Taken together, our results indicated that the prepared LFA has a strong potential to differentiate between AD patients and healthy controls, ensuring optimal patient management.

3.7 Stability of 4-MBA@AuNP-3G5 and dual-readout LFA

The storage stability of 4-MBA@AuNP-3G5 and LFA was further investigated. 4-MBA@AuNP-3G5 was stored in solid form at 4 °C for 60 days, while LFA was stored at room temperature for 60 days, and then their storage stability was tested separately. We first assessed the SERS signal of 4-MBA@AuNP-3G5 after storage. As shown in Fig. 7(d) and Fig. S9(a) in the ESM, characteristic bands were observed in 4-MBA@AuNP-3G5 before and after storage at 1,076 cm^{-1}, and the corresponding SERS intensity did not change significantly. In addition, the biological activity of 4-MBA@AuNP-3G5 before and after storage was evaluated by ELISA. The ELISA results showed that no significant change was observed before and after storage, and both of them could recognize p-tau^{396,404} (Fig. S9(b) in the ESM).

Furthermore, the stability of dual-readout LFA was investigated using different concentrations of p-tau^{396,404} protein. Figure 7(e) shows the visual results of LFA for the detection of low (60 pg/mL), medium (1,000 pg/mL), and high (4,000 pg/mL) concentrations of p-tau^{396,404} protein after 60 days of storage. The intensity of color and SERS increased with increasing p-tau^{396,404} concentration (Fig. S10 in the ESM and Fig. 7(f)). Notably, dual-readout LFA also showed positive results when p-tau^{396,404} protein concentration was 60 pg/mL by the naked eye, indicating the strong stability of LFA.

4 Conclusions

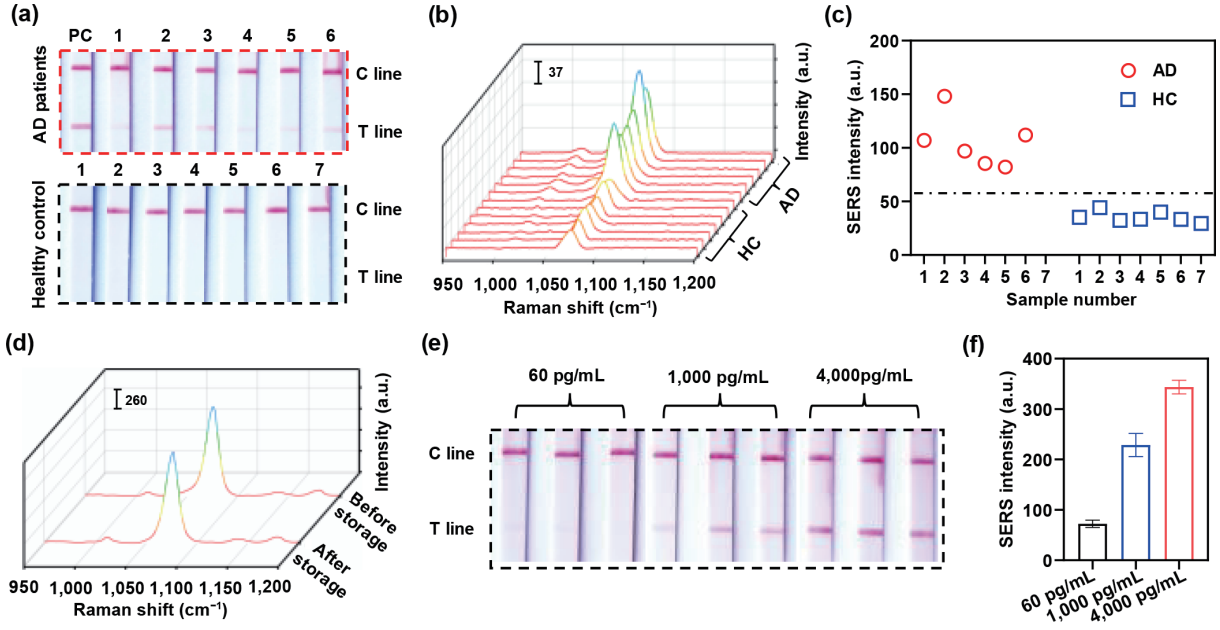

Figure 7 The actual detection capability of dual-readout LFA in human plasma samples. Visual results (a) and Raman spectra (b) of LFA in plasma samples of AD patients (n = 6) and health control (HC, n = 7). (c) The comparison of SERS-based LFA test results and the diagnosis results. (d) Raman spectra of 4-MBA@AuNP-3G5 before and after storage. Visual result (e) and SERS (f) intensity of dual-readout LFA detecting different concentrations of p-tau^{396,404} protein after storage. Data are presented as means ± SD, n = 3.

In this study, we first developed a colorimetric and SERS-based dual readout LFA to detect p-tau^{396,404}. LFA can be used for the rapid and quantitative detection of p-tau^{396,404} by SERS with a limit of quantification of 3.8 pg/mL and no cross-reactivity with other tau species. Besides, in colorimetric mode, LFA also allows visual judgment with a limit of quantification of 60 pg/mL. Results from mouse and clinical AD samples confirmed that the developed LFA has the feasibility and ability to rapidly detect p-tau^{396,404}, which is beneficial for the early diagnosis or enrichment of clinical trial populations of AD patients. It can further be used to monitor treatment effects, especially in the absence of PET or MRI imaging.

Acknowledgements

The authors would like to thank the technical support from Xuewei Du of the China University of Geosciences and Associate Professor Jinyang Zhang of Kunming University of Science and Technology in the screening of monoclonal antibodies. This study was financially supported by the National Science and Technology Innovation 2030 (Nos. 2021ZD0201000 and 2021ZD0201001), the National Natural Science Foundation of China (No. 81971025), and the Chinese Academy of Medical Sciences (CAMS) Innovation Fund for Medical Sciences (No. 2019-I2M-5-014). We also thank the Optical Bioimaging Core Facility and the Center for Nanoscale Characterization & Devices (CNCD) of WNLO-HUST, the Analytical and Testing Center of HUST, and the Research Core Facilities for Life Science (HUST) for support with data acquisition. We thank all patients and healthy individuals for donating their blood samples.

Electronic Supplementary Material: Supplementary material (characterization of AuNPs and 4-MBA@AuNP probe; the optimal 4-MBA load for AuNPs; the optimal K_2CO_3 volumes for 4-MBA@AuNP-3G5 conjugates; the optimal 3G5 load for 4-MBA@AuNP conjugates; effect of NaCl concentration on 4-MBA@AuNP-3G5 stability; the linear curve of T-line color and SERS intensity versus different p-tau^{396,404} concentrations; the comparison of colorimetric-based LFA test results and the diagnosis results; Raman intensities and antibody activity of 4-MBA@AuNP-3G5 before and after storage; colorimetric intensity of dual-readout LFA detecting different concentrations of p-tau^{396,404} protein; sequence of synthesized peptides used in this study; information of the participants in this study; the information of antibodies used in this study) is available in the online version of this article at https://doi.org/10.1007/s12274-022-5354-4.

References

[1] McDade, E.; Bateman. R. J. Stop Alzheimer's before it starts. *Nature* **2017**, *547*, 153–155.
[2] Lane, C. A.; Hardy, J.; Schott. J. M. Alzheimer's disease. *Eur. J. Neurol.* **2018**, *25*, 59–70.
[3] Scheltens, P.; De Strooper, B.; Kivipelto, M.; Holstege, H.; Chételat, G.; Teunissen, C. E.; Cummings. J.; van der Flier, W. M. Alzheimer's disease. *Lancet* **2021**, *397*, 1577–1590.
[4] GBD 2016 Dementia Collaborators. Global, regional, and national burden of Alzheimer's disease and other dementias. 1990-2016: A systematic analysis for the Global Burden of Disease Study 2016. *Lancet Neurol.* **2019**, *18*, 88–106.
[5] Ittner, L. M.; Götz. J. Amyloid-β and tau—A toxic *pas de deux* in Alzheimer's disease. *Nat. Rev. Neurosci.* **2011**, *12*, 65–72.
[6] Hardy, J. A.; Higgins. G. A. Alzheimer's disease: The amyloid cascade hypothesis. *Science* **1992**, *256*, 184–185.
[7] Giacobini, E.; Gold. G. Alzheimer disease therapy-moving from amyloid-β to tau. *Nat. Rev. Neurol.* **2013**, *9*, 677–686.
[8] Ballard, C.; Gauthier, S.; Corbett, A.; Brayne, C.; Aarsland, D.; Jones. E. Alzheimer's disease. *Lancet* **2011**, *377*, 1019–1031.
[9] Brazaca, L. C.; Moreto, J. R.; Martín, A.; Tehrani, F.; Wang, J.; Zucolotto. V. Colorimetric paper-based immunosensor for simultaneous determination of fetuin B and clusterin toward early Alzheimer's diagnosis. *ACS Nano* **2019**, *13*, 13325–13332.
[10] Zhang, L. D.; Liang, X. H.; Zhang, Z. H.; Luo. H. M. Cerebrospinal fluid and blood biomarkers in the diagnostic assays of Alzheimer's disease. *J. Innov. Opt. Health Sci.* **2022**, *15*, 2230001.
[11] Hu, S.; Yang, C. W.; Li, Y. Q.; Luo, Q. M.; Luo. H. M. Nanozyme sensor array based on manganese dioxide for the distinction between multiple amyloid β peptides and their dynamic aggregation process. *Biosens. Bioelectron.* **2022**, *199*, 113881.
[12] Mondragón-Rodríguez, S.; Perry, G.; Luna-Muñoz, J.; Acevedo-Aquino, M. C.; Williams. S. Phosphorylation of tau protein at sites

Ser$^{396-404}$ is one of the earliest events in Alzheimer's disease and Down syndrome. *Neuropathol. Appl. Neurobiol.* **2014**, *40*, 121–135.
[13] Gomes, L. A.; Uytterhoeven, V.; Lopez-Sanmartin, D.; Tomé, S. O.; Tousseyn, T.; Vandenberghe, R.; Vandenbulcke, M.; von Arnim, C. A. F.; Verstreken, P.; Thal. D. R. Maturation of neuronal AD-tau pathology involves site-specific phosphorylation of cytoplasmic and synaptic tau preceding conformational change and fibril formation. *Acta Neuropathol.* **2021**, *141*, 173–192.
[14] Ma, H.; Liu, S. L.; Liu, Y. W.; Zhu, J. Y.; Han, X. X.; Ozaki, Y.; Zhao. B. *In-situ* fingerprinting phosphorylated proteins via surface-enhanced Raman spectroscopy: Single-site discrimination of Tau biomarkers in Alzheimer's disease. *Biosens. Bioelectron.* **2021**, *171*, 112748.
[15] Shi, Y. C.; Gu, L. H.; Wang, Q.; Gao, L. J.; Zhu, J. L.; Lu, X.; Zhou, F. F.; Zhu, D.; Zhang, H. S.; Xie, C. M. et al. Platelet amyloid-β protein precursor (AβPP) ratio and phosphorylated tau as promising indicators for early Alzheimer's disease. *J. Gerontol. Ser. A* **2020**, *75*, 664–670.
[16] Fiandaca, M. S.; Kapogiannis, D.; Mapstone, M.; Boxer, A.; Eitan, E.; Schwartz, J. B.; Abner, E. L.; Petersen, R. C.; Federoff, H. J.; Miller, B. L. et al. Identification of preclinical Alzheimer's disease by a profile of pathogenic proteins in neurally derived blood exosomes: A case-control study. *Alzheimers Dement.* **2015**, *11*, 600–607.e1.
[17] Zhang, L.; Cao, K.; Su, Y; Hu, S.; Liang, X.; Luo, Q.; Luo, H. Colorimetric and surface-enhanced Raman scattering dual-mode magnetic immunosensor for ultrasensitive detection of blood phosphorylated tau in Alzheimer's disease. *Biosens Bioelectron.* **2023**, *222*, 114935.
[18] Ashton, N. J.; Pascoal, T. A.; Karikari, T. K.; Benedet, A. L.; Lantero-Rodriguez, J.; Brinkmalm, G.; Snellman, A.; Schöll, M.; Troakes, C.; Hye, A. et al. Plasma p-tau231: A new biomarker for incipient Alzheimer's disease pathology. *Acta Neuropathol.* **2021**, *141*, 709–724.
[19] Janelidze, S.; Mattsson, N.; Palmqvist, S.; Smith, R.; Beach, T. G.; Serrano, G. E.; Chai, X. Y.; Proctor, N. K.; Eichenlaub, U.; Zetterberg, H. et al. Plasma P-tau181 in Alzheimer's disease: Relationship to other biomarkers, differential diagnosis, neuropathology and longitudinal progression to Alzheimer's dementia. *Nat. Med.* **2020**, *26*, 379–386.
[20] Thambisetty, M.; Lovestone. S. Blood-based biomarkers of Alzheimer's disease: Challenging but feasible. *Biomark. Med.* **2010**, *4*, 65–79.
[21] Hampel, H.; O'Bryant, S. E.; Molinuevo, J. L.; Zetterberg, H.; Masters, C. L.; Lista, S.; Kiddle, S. J.; Batrla, R.; Blennow. K. Blood-based biomarkers for Alzheimer disease: Mapping the road to the clinic. *Nat. Rev. Neurol.* **2018**, *14*, 639–652.
[22] Foley, A. R.; Roseman, G. P.; Chan, K.; Smart, A.; Finn, T. S.; Yang, K.; Lokey, R. S.; Millhauser, G. L.; Raskatov. J. A. Evidence for aggregation-independent, PrP^{C}-mediated Aβ cellular internalization. *Proc. Natl. Acad. Sci. USA* **2020**, *117*, 28625–28631.
[23] Cintron, A. F.; Dalal, N. V.; Dooyema, J.; Betarbet, R.; Walker. L. C. Transport of cargo from periphery to brain by circulating monocytes. *Brain Res.* **2015**, *1622*, 328–338.
[24] Boluda, S.; Iba, M.; Zhang, B.; Raible, K. M.; Lee. V. M. Y.; Trojanowski, J. Q. Differential induction and spread of tau pathology in young PS19 tau transgenic mice following intracerebral injections of pathological tau from Alzheimer's disease or corticobasal degeneration brains. *Acta Neuropathol.* **2015**, *129*, 221–237.
[25] Clavaguera, F.; Grueninger, F.; Tolnay. M. Intercellular transfer of tau aggregates and spreading of tau pathology: Implications for therapeutic strategies. *Neuropharmacology* **2014**, *76*, 9–15.
[26] Guo, J. L.; Lee. V. M. Y. Cell-to-cell transmission of pathogenic proteins in neurodegenerative diseases. *Nat. Med.* **2014**, *20*, 130–138.
[27] Ye, L.; Hamaguchi, T.; Fritschi, S. K.; Eisele, Y. S.; Obermüller, U.; Jucker, M.; Walker. L. C. Progression of seed-induced Aβ deposition within the limbic connectome. *Brain Pathol.* **2015**, *25*, 743–752.
[28] Lakshmi, S.; Essa, M. M.; Hartman, R. E.; Guillemin, G. J.; Sivan, S.; Elumalai. P. Exosomes in Alzheimer's disease: Potential role as pathological mediators, biomarkers and therapeutic targets. *Neurochem. Res.* **2020**, *45*, 2553–2559.
[29] Jia, L. F.; Qiu, Q. Q.; Zhang, H.; Chu, L.; Du, Y. F.; Zhang, J. W.; Zhou, C. K.; Liang, F. R.; Shi, S. L.; Wang, S. et al. Concordance between the assessment of Aβ42, T-tau, and P-T181-tau in peripheral blood neuronal-derived exosomes and cerebrospinal fluid. *Alzheimers Dement.* **2019**, *15*, 1071–1080.
[30] Barthélemy, N. R.; Horie, K.; Sato, C.; Bateman. R. J. Blood plasma phosphorylated-tau isoforms track CNS change in Alzheimer's disease. *J. Exp. Med.* **2020**, *217*, e20200861.
[31] Thijssen, E. H.; La Joie, R.; Wolf, A.; Strom, A.; Wang, P.; Iaccarino, L.; Bourakova, V.; Cobigo, Y.; Heuer, H.; Spina, S. et al. Diagnostic value of plasma phosphorylated tau181 in Alzheimer's disease and frontotemporal lobar degeneration. *Nat. Med.* **2020**, *26*, 387–397.
[32] Hanger, D. P.; Anderton, B. H.; Noble. W. Tau phosphorylation: The therapeutic challenge for neurodegenerative disease. *Trends Mol. Med.* **2009**, *15*, 112–119.
[33] Liu, L.; Kwak, H.; Lawton, T. L.; Jin, S. X.; Meunier, A. L.; Dang, Y. F.; Ostaszewski, B.; Pietras, A. C.; Stern, A. M.; Selkoe. D. J. An ultra-sensitive immunoassay detects and quantifies soluble Aβ oligomers in human plasma. *Alzheimers Dement.* **2022**, *18*, 1186–1202.
[34] Palmqvist, S.; Janelidze, S.; Quiroz, Y. T.; Zetterberg, H.; Lopera, F.; Stomrud, E.; Su, Y.; Chen, Y. H.; Serrano, G. E.; Leuzy, A. et al. Discriminative accuracy of plasma phospho-tau217 for Alzheimer disease vs other neurodegenerative disorders. *JAMA* **2020**, *324*, 772–781.
[35] Liu, Y. L.; Zhan, L.; Qin, Z. P.; Sackrison, J.; Bischof. J. C. Ultrasensitive and highly specific lateral flow assays for point-of-care diagnosis. *ACS Nano* **2021**, *15*, 3593–3611.
[36] Ren, W.; Mohammed, S. I.; Wereley, S.; Irudayaraj. J. Magnetic focus lateral flow sensor for detection of cervical cancer biomarkers. *Anal. Chem.* **2019**, *91*, 2876–2884.
[37] Ruppert, C.; Kaiser, L.; Jacob, L. J.; Laufer, S.; Kohl, M.; Deigner. H. P. Duplex Shiny app quantification of the sepsis biomarkers C-reactive protein and interleukin-6 in a fast quantum dot labeled lateral flow assay. *J. Nanobiotechnol.* **2020**, *18*, 130.
[38] Kim, H. M.; Kim, J.; An, J.; Bock, S.; Pham, X. H.; Huynh, K. H.; Choi, Y.; Hahm, E.; Song, H.; Kim, J. W. et al. Au-Ag assembled on silica nanoprobes for visual semiquantitative detection of prostate-specific antigen. *J. Nanobiotechnol.* **2021**, *19*, 73.
[39] Liu, Q. Y.; Cheng, S. M.; Chen, R.; Ke, J. M.; Liu, Y. W.; Li, Y. F.; Feng, W.; Li. F. Y. Near-infrared lanthanide-doped nanoparticles for a low interference lateral flow immunoassay test. *ACS Appl. Mater. Interfaces* **2020**, *12*, 4358–4365.
[40] Ji, T. X.; Xu, X. Q.; Wang, X. D.; Cao, N.; Han, X. R.; Wang, M. H.; Chen, B.; Lin, Z.; Jia, H. Y.; Deng, M. et al. Background-free chromatographic detection of sepsis biomarker in clinical human serum through near-infrared to near-infrared upconversion immunolabeling. *ACS Nano* **2020**, *14*, 16864–16874.
[41] Xu, K. C.; Zhou, R.; Takei, K.; Hong, M. H. Toward flexible surface-enhanced Raman scattering (SERS) sensors for point-of-care diagnostics. *Adv. Sci. (Weinh.)* **2019**, *6*, 1900925.
[42] Madzharova, F.; Heiner, Z.; Kneipp. J. Surface enhanced hyper Raman scattering (SEHRS) and its applications. *Chem. Soc. Rev.* **2017**, *46*, 3980–3999.
[43] Xia, C.; Zhang, D.; Li, H.; Li, S.; Liu, H.; Ding, L.; Liu, X.; Lyu, M.; Li, R.; Yang, J. et al. Single-walled carbon nanotube based SERS substrate with single molecule sensitivity. *Nano Research.* **2022**, *15*, 694–700.
[44] Shi, L. L.; Xu, L.; Xiao, R. H.; Zhou, Z.; Wang, C. W.; Wang, S. Q.; Gu, B. Rapid, quantitative. high-sensitive detection of *Escherichia coli* O157: H7 by gold-shell silica-core nanospheres-based surface-enhanced Raman scattering lateral flow immunoassay. *Front. Microbiol.* **2020**, *11*, 596005.
[45] Fu, X. L.; Wen, J. H.; Li, J. W.; Lin, H.; Liu, Y. M.; Zhuang, X. M.; Tian, C. Y.; Chen. L. X. Highly sensitive detection of prostate cancer specific PCA3 mimic DNA using SERS-based competitive lateral flow assay. *Nanoscale* **2019**, *11*, 15530–15536.
[46] Tian, M.; Wang, J.; Li, C.; Wang, Z.; Liu, G.; Lv, E.; Zhao, X.; Li, Z.; Cao, D.; Liu, H. et al. Qualitative and quantitative detection of

microcystin-LR based on SERS-FET dual-mode biosensor. *Biosens Bioelectron.* **2022**, *212*, 114434.

[47] Kim, K.; Han, D. K.; Choi, N.; Kim, S. H.; Joung, Y.; Kim, K.; Ho, N. T.; Joo, S. W.; Choo. J. Surface-enhanced Raman scattering-based dual-flow lateral flow assay sensor for the ultrasensitive detection of the thyroid-stimulating hormone. *Anal. Chem.* **2021**, *93*, 6673–6681.

[48] Cheng, N.; Lou, B.; Wang. H. An intelligent serological SERS test toward early-stage hepatocellular carcinoma diagnosis through ultrasensitive nanobiosensing. *Nano Research.* **2022**, *15*, 5331–5339.

[49] Liang, J. J.; Teng, P. J.; Xiao, W.; He, G. B.; Song, Q. F.; Zhang, Y.; Peng, B.; Li, G.; Hu, L. S.; Cao, D. L. et al. Application of the amplification-free SERS-based CRISPR/Cas12a platform in the identification of SARS-CoV-2 from clinical samples. *J. Nanobiotechnol.* **2021**, *19*, 273.

[50] Perrault, S. D.; Chan, W. C. W. Synthesis and surface modification of highly monodispersed. spherical gold nanoparticles of 50-200 nm. *J. Am. Chem. Soc.* **2009**, *131*, 17042–17043.

[51] Zhang, L. D.; Du, X. W.; Su, Y.; Niu, S. Q.; Li, Y. Q.; Liang, X. H.; Luo. H. M. Quantitative assessment of AD markers using naked eyes: Point-of-care testing with paper-based lateral flow immunoassay. *J. Nanobiotechnol.* **2021**, *19*, 366.

[52] Zhang, L. D.; Yang, C. W.; Li, Y. Q.; Niu, S. Q.; Liang, X. H.; Zhang, Z. H.; Luo, Q. M.; Luo. H. M. Dynamic changes in the levels of amyloid-β_{42} species in the brain and periphery of APP/PS1 mice and their significance for Alzheimer's disease. *Front. Mol. Neurosci.* **2021**, *14*, 723317.

[53] Qu, W.; Zhang, L.; Liang, X.; Yu, Z.; Huang, H.; Zhao, J.; Guo, Y.; Zhou, X.; Xu, S.; Luo, H. et al. Elevated plasma oligomeric amyloid β-42 is associated with cognitive impairments in cerebral small vessel disease. *Biosensors (Basel).* **2023**, *13*, 110.

[54] Abramoff, M. D.; Magelhaes, P. J.; Ram. S. J. Image processing with ImageJ. *Biophotonics Int.* **2004**, *11*, 36–42.

[55] Zhang, L. D.; Du, X. W.; Chen, Z. X.; Chen, C. J.; Gong, N. X.; Song, Y. H.; Song, Y. Z.; Han, Q. Q.; Xia, X. S.; Luo, H. M. et al. Instrument-free and visual detection of salmonella based on magnetic nanoparticles and an antibody probe immunosensor. *Int. J. Mol. Sci.* **2019**, *20*, 4645.

[56] Hu, Y. Y.; He, S. S.; Wang, X. C.; Duan, Q. H.; Grundke-Iqbal, I.; Iqbal, K.; Wang. J. Z. Levels of nonphosphorylated and phosphorylated tau in cerebrospinal fluid of Alzheimer's disease patients: An ultrasensitive bienzyme-substrate-recycle enzyme-linked immunosorbent assay. *Am. J. Pathol.* **2002**, *160*, 1269–1278.

[57] Phan, L. M. T.; Cho. S. Fluorescent aptasensor and colorimetric aptablot for p-tau231 detection: Toward early diagnosis of Alzheimer's disease. *Biomedicines* **2022**, *10*, 93.

[58] Luk, C.; Giovannoni, G.; Williams, D. R.; Lees. A. J.; de Silva, R. Development of a sensitive ELISA for quantification of three- and four-repeat tau isoforms in tauopathies. *J. Neurosci. Methods* **2009**, *180*, 34–42.